



## Seasonal cycle of desertic aerosols in West Africa : Analysis of the Coastal transition with passive and active sensors

Habib Senghor<sup>1</sup>, Éric Machu<sup>1,2</sup>, Frédéric Hourdin<sup>3</sup>, and Amadou Thierno Gaye<sup>1</sup>

<sup>1</sup>Laboratoire de Physique de l'Atmosphère et de l'Océan Siméon-Fongang (LPAO-SF), École Supérieure Polytechnique (ESP) de l'Université Cheikh Anta Diop de Dakar (UCAD), Sénégal

<sup>2</sup>Laboratoire de Physique des Océans (LPO), Institut Universitaire Européen de la Mer (IUEM), Brest, France

<sup>3</sup>Laboratoire de Météorologie Dynamique (LMD), CNRS/IPSL/UMPC, Paris, France

*Correspondence to:* H. Senghor (habib.senghor@ird.fr)

1 **Abstract.** The impact of desertic aerosols on climate, atmospheric processes and the environment is still debated in the sci-  
2 entific community. The extent of their influence remains to be determined and particularly requires a better understanding of the  
3 variability of their distribution. In this work, we studied the variability of these aerosols in West Africa using different types of  
4 satellite observations. SeaWiFS and OMI data have been used to characterize the spatial distribution of mineral aerosols from  
5 their optical and physical properties over the period 2005-2010. In particular, we focused on the variability of the transition  
6 between the West African continent and the Eastern Atlantic Ocean. Data provided by the Lidar scrolling CALIOP onboard the  
7 satellite CALIPSO (Cloud Aerosol Lidar and Infrared Pathfinder Satellite Observations) for the period 2007-2013 were then  
8 used to assess the seasonal variability of the vertical distribution of desertic aerosols. We first obtained a good representation  
9 of Aerosol Optical Depth (AOD) and Single Scattering Albedo (SSA) by satellites (SeaWiFS and OMI, respectively) in com-  
10 parison with AERONET estimates, both above the continent and the ocean. Dust occurrence frequency is higher in spring and  
11 boreal summer. In spring, the highest occurrences are located between the surface and 3 km above sea level, while in summer  
12 the highest occurrences are between 2 and 5 km altitude. The vertical distribution given by CALIOP also highlights an abrupt  
13 change at the coast from spring to fall with a layer of desertic aerosols confined in an atmospheric layer uplifted from the  
14 surface of the ocean. This uplift of the aerosol layer above the ocean contrasts with the winter season during which mineral  
15 aerosols are confined in the atmospheric boundary layer. Radiosondes at Dakar Weather Station (17.5°W, 14.74°N) provide  
16 basic thermodynamic variables which partially give causal relationship between the layering of the atmospheric circulation  
17 over West Africa and their aerosol contents throughout the year. A SSA increase is observed in winter and spring at the tran-  
18 sition between the continent and the ocean. The analysis of mean NCEP winds at 925 hPa between 2000 and 2012 suggest a  
19 significant contribution of coastal sand sources from Mauritania in winter which would increase SSA over the ocean.



## 20 1 Introduction

21 The Sahara is the largest source of mineral aerosols in the world, with a contribution of almost 40% compared to the overall  
22 emissions from natural sources (Ramanathan et al., 2001; Tanaka et al., 2005). These minerals and desert aerosols are emitted  
23 in arid and semi-arid North Africa and transported across the Atlantic Ocean to the American continent, the Caribbean islands,  
24 Florida (Chiapello et al., 1995; Dunion and Marron, 2008), South America (Prospero et al., 1981; Liu et al., 2008, 2012) and  
25 North America (Tsamalis et al., 2013). They play a very important role on the climate and the various processes involved  
26 in the climate system (Kaufman et al., 2005; Teller and Levin, 2006; Stith et al., 2009) through their direct impact in the  
27 visibility, in the infrared (Sokolik and Toon, 1999) or the earth radiation budget (Andreae et al., 1996; Solomon, 2007) which  
28 is still poorly known. The difficulty of understanding the impact of aerosols on the Earth's radiation balance is due to the large  
29 spatial and temporal variability of their concentration and composition in the atmosphere. The mineral particles suspended in  
30 the atmosphere come from different sources and have a nature similar to the nature of the soil from which they arise (Claquin  
31 et al., 1999; Formenti et al., 2008) with a broad spectrum of particle sizes ranging between 0.01 and 100 micrometers (Wagener,  
32 2008). Their impact on the marine ecosystem and particularly on oceanic primary production (Duce and Tindale, 1991; Baker  
33 et al., 2003; Mills et al., 2004; Jickells et al., 2005; Mahowald et al., 2009) remains still uncertain and difficult to assess because  
34 of the composition of these particles and of physico-chemical processes affecting them (e.g., Friese et al., 2016). Mineral dust  
35 deposition also have a negative impact on human health and are responsible for meningitis epidemics or cardiac diseases  
36 (Thomson et al., 2006; Martiny and Chiapello, 2013; Diokhane et al., 2016; Prospero et al., 2005; Griffin, 2007).

37 The desert aerosols and their large-scale transport began to be studied in the 90s from satellite observations (Husar et al.,  
38 1997; Moulin, 1997). Passive sensors have the advantage of providing daily data on the state of the atmosphere with good  
39 spatial and temporal coverage. The satellite products have improved our knowledge of the source regions and dust transport  
40 pathways in recent years (Engelstaedter et al., 2006). However, studies of their spatial and temporal variability are mainly  
41 based on indices such as the Aerosol Optical Depth (AOD) or the Aerosol Index (AI) which provide vertically integrated  
42 information on the Atmospheric aerosol contents (passive space derived observations: (Cakmur et al., 2001; Chiapello and  
43 Moulin, 2002; Kaufman et al., 2005; Engelstaedter et al., 2006; Schepanski et al., 2009b). These satellite products also present  
44 some limitations since they are unable to differentiate aerosols and particularly those from desertic origin. Moreover AOD  
45 estimated by satellite integrates the contribution of every kind of particles and this latter estimation also depends on the altitude  
46 at which aerosols are located. In other words the signal changes with the height of the aerosol plume for a given aerosol content  
47 (Chiapello et al., 1999).

48 Recently, the vertical structure of the SAL has been analyzed from CALIPSO satellite observations. The vertical disconnection  
49 of dust layers between land and ocean strongly impacts the atmospheric deposition rates of mineral matters (Schepanski et al.,  
50 2009a) and dust concentration at the oceanic surface which has important consequences on the primary biological productivity  
51 of surface waters (Martin, 1992; Arístegui et al., 2009).

52 In boreal summer, the Saharan Air Layer (SAL) is characterized by hot, dry air, very dust-laden and is located between 10°N  
53 and 25°N (Dunion and Marron, 2008; Tsamalis et al., 2013). This SAL is marked by very strong potential temperatures up to



54 40°C and a radon presence (radon-222) indicating the desert origin of air masses (Carlson and Prospero, 1972).  
55 In winter, the SAL is characterized by the transport of chemical elements such as aluminum (Al), silicon (Si), iron (Fe), titanium  
56 (Ti) and manganese (Mn) ( e.g., Ben-Ami et al., 2010) and is located between 5°N and 10°N ( e.g., Tsamalis et al., 2013). The  
57 studies relating aerosols to their transport are generally a simple description of the vertical distribution of aerosols in the SAL  
58 (Generoso et al., 2008; Liu et al., 2008; Ben-Ami et al., 2009; Braun, 2010; Yu et al., 2010; Adams et al., 2012; Ridley et al.,  
59 2012; Yang et al., 2012) or a description of the seasonality of the SAL in connection with large-scale dynamics (Liu et al.,  
60 2012; Tsamalis et al., 2013). The effects of small-scale dynamics and thermodynamics for controlling the vertical structure of  
61 desert aerosols in coastal West Africa remain unknown, and efforts made in this direction are restricted to very sporadic case  
62 studies (Gamo, 1996; Reid et al., 2002; Petzold et al., 2011).

63 In this study, in-situ and satellite observations are used to describe the seasonal time-scale of mineral dust distribution. We first  
64 used complementary information, provided by Sea-viewing Wide Field Sensor (SeaWiFS) and Ozone Monitoring Instrument  
65 (OMI) which deliver optical (AOD: Aerosol Optical Depth; SSA: Single Scattering Albedo) and physical (AE: Angstrom  
66 Exponent) properties of desertic aerosols, to analyse the spatial variability of the desertic aerosol dust. Then we used CALIOP  
67 lidar on board CALIPSO to investigate the vertical distribution of these desertic aerosols.

68 We finally analyze meteorological data to explain the impact of the atmospheric variables on the seasonal cycle of the vertical  
69 distribution of desertic aerosols at the transition zone between the continent and the ocean. We conclude the present work by  
70 summarizing all the results which are reflecting our common knowledge on mineral dust discrimination and spatio-temporal  
71 distribution.

## 72 **2 Methodology and Data**

### 73 **2.1 AEROSOL ROBOTIC NETWORK (AERONET)**

74 We first used data of AOD from AERONET between January 2005 and December 2010. AERONET is a global network of in-  
75 situ observations developed by the NASA Earth Observing System (NASA's EOS) (Dubovik et al., 2000). AERONET consists  
76 of solar photometers Cimel providing measures of AOD every 15 minutes, refractive index and also allows inversions such as  
77 particle size distribution of aerosols and single scattering albedo (SSA) at 440nm, 670nm, 870nm and 1020nm wavelengths  
78 (Holben et al., 1998) with an accuracy of  $\pm 0.01$  (Slutsker and Kinne, 1999; Dubovik et al., 2000; Holben et al., 2001).  
79 AERONET's SSA are computed for favorable atmospheric conditions (AOD 440 nm > 0.4 and solar zenith angle >45°) using  
80 an algorithm which performs almucantar inversions (Jethva et al., 2014). These data are used to validate remotely sensed AOD  
81 and SSA measurements.

### 82 **2.2 Sea-viewing Wide Field-of-view Sensor (SeaWiFS)**

83 We then used DeepBlue-SeaWiFS monthly mean AOD at 550 nm and AE products derived from SeaWiFS developed by NASA  
84 to study ocean color. SeaWiFS measures the solar radiation reflected at the top of the atmosphere in the wavelengths 412 nm,



85 443 nm, 490 nm, 510 nm, 555 nm, 670 nm, 765 nm and 865 nm. Satellite measurements carried out between October 1997  
86 and December 2010 (Jamet et al., 2004; Hsu et al., 2012) have a value of signal-to-noise and uncertainty of 2%-3% for the  
87 different spectral bands (for details see (Eplee et al., 2007; Franz et al., 2007; Eplee Jr et al., 2011)). In this paper, we use the  
88 Level 3 version 4 products (Bettenhausen and Team, 2013) for years 2005 to 2010. The SeaWiFS AOD provided at 550 nm is  
89 available both over the land and over the ocean (Hsu et al., 2004; Sayer et al., 2012). The products used here are land-ocean  
90 estimates generated and made available to the scientific community by NASA (Wang et al., 2000).

### 91 2.3 Ozone Monitoring Instrument (OMI)

92 OMI is a passive sensor on board the Aura satellite launched on 15 July 2004 by NASA's EOS Aura space-craft which released  
93 its first observations in October 2004. Like all satellites in the A-Train constellation, OMI scans the entire Earth in 14 to 15  
94 orbits with a nadir ground pixel spatial resolution of  $13 \times 24 \text{ km}^2$  (Jethva et al., 2014). In addition to the ozone content in the  
95 atmosphere OMI provides information on aerosols, clouds, gases ( $\text{NO}_2$ ,  $\text{SO}_2$ , HCHO, BrO, and OCIO) and irradiance in the  
96 ultraviolet (Levelt et al., 2006). We use Aura/OMI SSA at 500 nm taken from the OMAERUV Level 3 Collection 003 aerosol  
97 product processed in March 2012 with a spatial resolution of  $1^\circ \times 1^\circ$  to quantify the scattering of the aerosol types with passive  
98 sensors. The OMAERUV algorithm assigns flag to each pixel which carries information on the quality of the retrieval (Jethva  
99 et al., 2014).

100 The SSA represents the ratio (ranging between 0 and 1) of scattering coefficient to extinction coefficient and provides infor-  
101 mation about the absorbing properties of the aerosols. SSA of 0.9 indicates that 90% of the total extinction of solar light is  
102 caused by scattering and 10% by absorption effects (Jethva et al., 2014). This parameter depends on the wavelength, size and  
103 the complex refractive index of particles (Léon et al., 2009). The closer this value is to one the more desert aerosols dominate  
104 (Johnson et al., 2008; Léon et al., 2009; Ialongo et al., 2010; Malavelle, 2011).

105 OMI data were interpolated on the grid of SeaWiFS data to superimpose the products (AOD and SSA).

### 106 2.4 Cloud Aerosol Lidar and Infrared Pathfinder Satellite Observations (CALIPSO)

107 The first polarization lidar in space so-called CALIPSO is a sun-synchronous satellite developed by NASA as part of the Earth  
108 System Science Pathfinder program (ESSP) and launched on April 28, 2006 (Winker et al., 2007; Hunt et al., 2009) in order  
109 to provide a global coverage of the vertical distribution of the properties of clouds and aerosols (Winker, 2003). The lidar  
110 (LIght Detection and Ranging) Cloud-Aerosol Backscatter Lidar with Orthogonal Polarization (CALIOP) onboard CALIPSO  
111 acquires vertical profiles of the atmosphere at 30 m resolution in the lower layers (from the two orthogonal components that  
112 result from depolarization of a signal backscattered laser at 532 nm and vertical profiles of a total laser at 1064 nm signal  
113 backscattered at nadir). The final level-2 product is reduced to a uniform resolution calculated from averaging and/or inter-  
114 polating different resolutions for generating intermediate products (Winker et al., 2006). We use the Vertical Feature Mask  
115 (VFM; stage 1 Version 3) for which the processing algorithm is described in CALIOP Algorithm Theoretical Basis, Part 3:  
116 Scene Algorithms Classification (Liu et al., 2005). VFM allows to separate aerosols from clouds but also the desert aerosols  
117 from other types of aerosols (Omar et al., 2009). This methodology of discrimination by CALIOP of aerosol types gives results



118 close to another method of distinction between mineral dust made from inversions (SSA and AE) of AERONET level 2 prod-  
119 ucts (Mielonen et al., 2009). The mix of layers of desert aerosol and other types of aerosols (i.e. biomass burning) is very rare  
120 (Chou et al., 2008; Heese and Wiegner, 2008) in our region of interest. During the dry season, mineral aerosols are observed  
121 in the atmospheric surface layer ranging 0.5 to 1 km while the aerosol emitted through biomass burning are carried to higher  
122 levels up to 5 km altitude (Cavalieri et al., 2010). Nevertheless, classification errors are possible for low values of the Mineral  
123 Dust Occurrence Frequency (MDOF) and at frontal zones between layers of different substances (Adams et al., 2012). For this  
124 reason we only consider here the values of MDOF above 10%. Our method for determining the mineral dust by a calculation  
125 of the MDOF is equivalent to (Adams et al., 2012) expressed by the following equation:

126

$$127 \quad p(x, y, z) = \frac{\sum_{n=0}^N p(x+n, y, z)}{\sum_{n=0}^N s(x+n, y, z)} \quad \forall \quad x, y, z \quad (1)$$

128

129

130 where  $p$  is the probability of occurrence of dust at a grid point,  $s$  the total number of valid satellite passing the same grid  
131 point and  $N$  the total number of grid points. Data were gridded with a near-uniform horizontal resolution of  $0.5^\circ \times 0.5^\circ$  and a  
132 vertical resolution of 30 m for 290 vertical levels between 0.5 and 8.2 km above sea level. The CALIOP lidar on CALIPSO  
133 (also in the A-train) has a 90 m instantaneous footprint which is smeared to 333 m in the along track direction by orbital  
134 motion over the lidar pulse duration. All satellites of the A-train constellation, such as CALIPSO, fly in a sun-synchronous  
135 orbit with a 16 days coverage cycle consisting of 233 orbits separated by 1.54 degrees longitude or about 172 km at the equator.  
136 Each satellite completes 14.55 orbits per day with a separation of 24.7 degrees longitude between each successive orbit at the  
137 equator. These CALIPSO orbits are controlled to cover the same ground with cross-track errors of less than  $\pm 10$  km (Winker  
138 et al., 2007). This drastically reduces the spatial coverage of the satellite. Consequently, we use a mesh of  $0.5^\circ$  longitude to  
139 cover the area between  $10^\circ\text{W}$ - $24^\circ\text{W}$  and  $12^\circ\text{N}$ - $21^\circ\text{N}$ . The choice of this band of latitude is driven by one of the objectives of  
140 the paper which is to study the transition of aerosol distribution between the continent and the ocean. Dust occurrences are  
141 averaged over latitudes  $12^\circ\text{N}$  to  $21^\circ\text{N}$  and are then smoothed over 30 points longitudinal running mean and 50 points vertical  
142 running mean.

### 143 3 Results

#### 144 3.1 Horizontal dust distribution

145 SeaWiFS AOD (estimated at wavelength 550 nm) represents an average value of the optical Depth of the atmosphere. It has first  
146 been compared to the monthly AOD given by AERONET photometers (given at the wavelength 675 nm) by calculating the cor-



147 relation between the two measurements at different selected stations (Fig. 1). Our choice focused on the stations Banizoumbou  
148 (2.665°E-13.541°N), Agoufou (1.479°W-15.345°N), M'bour (16.959°W-14.394°N) and Capo Verde (22.935°W-16.733°N) to  
149 assess the quality of satellite information obtained across the land-ocean continuum. A very good correlation is calculated be-  
150 tween SeaWiFS and in-situ measurement given by the photometer at Banizoumbou ( $R=0.95$ ; Fig. 1a). The photometer Cimel  
151 at Agoufou (Mali) also shows a very good correlation with SeaWiFS ( $R=0.92$ ; Fig. 1b). The correlation between the two  
152 measures is equal to 0.81 at the shore in M'bour (Fig. 1c). It is close to the one in Capo Verde ( $R=0.83$ ; Fig. 1d). All these  
153 correlation values of AOD are significant at 95% using a student statistical test. We also studied the structure of the cloud of  
154 points between the two datasets to assess the quality of the satellite measurements as a function of the aerosol concentration.  
155 The regression line obtained by the least squares method shows a linear relationship between satellite and in-situ monthly mean  
156 measurements of AOD at the selected stations.

157 The horizontal transport of desert aerosols can be followed by considering the key and complementary parameters that dis-  
158 tinguish them. To better characterize the desertic aerosols, we combined AOD (SeaWiFS) with SSA (OMI) to specify the  
159 contribution of the latter compared to other types of aerosols in the atmosphere. A threshold of 0.90 in monthly averaged SSA  
160 is used to define regions dominated by desert aerosols. This value is chosen in agreement with the threshold value given in  
161 previous studies (Léon et al., 2009; Malavelle, 2011; Jethva et al., 2014). This method allowed us to define the Sahelo-Saharan  
162 region as the one which is the most influenced by dust plumes composed of desert aerosols throughout the year (between 12°N  
163 and 21°N; Fig. 3).

164 The comparison of the daily SSA of Aura/OMI versus AERONET is achieved to validate satellite SSA which provides  
165 a better spatio-temporal coverage of our region of interest. OMI SSA retrievals are taken between 10 and 15 am <https://ozoneaq.gsfc.nasa.gov/data/lance-browse/>, time range which cover AERONET measurements. As emphasized by Jethva et al.  
166 (2014), this comparison is done at the original wavelengths of each independent measurement (388 nm for OMI and 438 nm for  
167 AERONET) in order to avoid uncertainties induced by the interpolation at other wavelengths. Good correlations are retrieved  
168 between the two datasets at the different ground stations in West Africa for the period 2005-2010 within root mean square  
169 (RMS) difference of 0.03 in the selected region (Fig. 2). Globally, the OMAERUV SSA is well correlated with ground mea-  
170 surements. The correlation at all selected sites for this study is significant. The agreement between the two inversions is better  
171 at the shore of West Africa (M'bour station:  $r=0.66$ ) and over the ocean (Capo Verde station:  $r=0.30$ ) than over the continent  
172 (Banizoumbou station,  $r=0.47$  and Agoufou station:  $r=0.50$ ).

174 Figure 3 and Figure 4 show that horizontal monthly average of AOD is stronger above the continent than over the ocean  
175 throughout the year. The weakest AOD is given for winter months (DJF for December-January-February) with a mean value of  
176  $0.33 \pm 0.07$  (standard deviation). At this season, the SSA values are higher in the northeast tropical Atlantic than on the West  
177 African continent with a SSA maximum reaching 0.95. This indicates a stronger contribution of dust over the ocean than over  
178 the continent in the latitude range 12°N-21°N. Note that sources of dust aerosols are also indicated by high SSA values north  
179 of 21°N.

180 In spring (MAM for March-April-May), the increase of the monthly mean AOD compared to winter is indicated by a stronger  
181 mean value ( $0.50 \pm 0.08$ ). The mean optical depth indicates that the dust sources are becoming more active with an atmosphere





182 more charged than in winter. The coarse mode dominates in the mixed atmosphere boundary layer over the continent with  
183 lower values of AE less than 0.7 (not shown). Nevertheless, the reflectance properties of aerosols (given by the SSA) is higher  
184 over the ocean than over the continent and vary weakly compared to winter.

185 In summer (JJA for June-July-August), the maximum mean AOD is  $0.52 \pm 0.05$ . AOD values are associated with higher SSA  
186 above 0.96. It indicates that aerosols are clearly dominated by desert dust in boreal summer. At this season, the largest dust  
187 particles are mobilized and raised above the continent by convective systems (e.g., Rajot, 2001, Fig. 4c).

188 In autumn (SON for September-October-November), the monthly mean AOD is  $0.34 \pm 0.05$ . AOD is decreased compared to  
189 spring but the SSA values are much higher than in spring despite the fact that uplift occurrences are larger in spring than in fall  
190 in west Africa (Marticorena et al., 2010; Diokhane et al., 2016).

191 Changes of AOD and SSA are seen at the transition between the continent and the ocean (Fig. 4). Understanding these changes  
192 requires a thorough analysis of the vertical distribution of dust during transportation from east to west in North Africa.

### 193 3.2 Vertical dust distribution

194 The vertical distribution of desert aerosol indicates a strong presence of dust concentrations between the surface and 6 km in  
195 agreement with the results of Léon et al. (2009) who studied the vertical distribution of dust in the North-East Tropical Atlantic  
196 (Fig. 5).

197 In DJF, desert aerosols are mainly concentrated in the atmospheric boundary layer (ABL) between the surface and 2 km  
198 (Fig. 5a) both over the continent and the ocean. At this season, we also noted a homogeneous dust aerosol transition between  
199 Western Africa and the Eastern part of the Atlantic Ocean.

200 In MAM, there is an elevation of the SAL with a maximum altitude of 5 km on the continent and between 4 and 5 km above  
201 the ocean (Fig. 5b). The MDOF over 50% above the continent shows that dust emissions are much greater than in winter. ABL  
202 develops vertically to reach the level of the SAL. It results in an atmospheric layer well mixed between the surface and 5 km  
203 of altitude above the continent ( $10^{\circ}\text{W}$ - $15^{\circ}\text{W}$ ). Above the Ocean we see a detachment of the SAL from the ocean surface which  
204 occurs at the coast (around  $18^{\circ}\text{W}$ ).

205 JJA is the busiest season of the year in terms of dust rising in the northern hemisphere of Africa. It is characterized by the de-  
206 velopment of density currents that intensify the mobilization of terrigenous aerosols (e.g., Bou Karam et al., 2008; Schepanski  
207 et al., 2009b, Fig. 5c).

208 Unlike DJF, we note a clear separation of the dust layer above the Eastern Atlantic Ocean where dusts are confined between 1  
209 and 6 km altitude.

210 In SON, dust emissions decrease in intensity compared to JJA but the detachment from the surface of the ocean remains clear  
211 at the coast although less marked than in JJA (Fig. 5d). According to Adams et al. (2012), the heart of the SAL is located about  
212 5 km above sea level in SON, whereas Liu et al. (2012) shows a maximum altitude of 4 km.



## 213 4 Discussion

### 214 4.1 Seasonal variability

215 The desert aerosols in the band of latitude  $12^{\circ}\text{N}$ - $21^{\circ}\text{N}$  are mainly emitted in the Saharan and Sahelian regions. Emissions and  
216 transport processes are mainly controlled by meteorological variables (Brooks and Legrand, 2000; Joseph, 1999).

217 In the Sahara, the sources of dust emissions are less active in winter than during the other seasons and the vertical distribution  
218 of aerosols is not supported by a favorable wind regime ascending particles. The maximum altitude of this distribution is 3  
219 km above the continent and 2 km at the West African coast in agreement with the studies of (Léon et al., 2009) and (Vuolo  
220 et al., 2009). Compared to other seasons, DJF show an important role played by the shallower atmospheric layers on the dust  
221 transported from source regions located in the Northwestern part of Mauritania and more generally in the West African coastal  
222 region (Fig. 6a). These West African emission zones participate actively to the transport of mineral aerosols in the near Atlantic  
223 Ocean. This high occurrence is shown by the inter-seasonal variability derived from NCEP Reanalysis. Figure. 6 highlights  
224 that the Northwest region of Mauritania has the highest standard deviation of horizontal wind intensity between  $18^{\circ}\text{N}$ - $24^{\circ}\text{N}$   
225 and that wind is very intense in winter compared to the other seasons (Fig. 6a). Hence this region represents an important sand  
226 source in winter as mentioned by previous studies (Bertrand et al., 1979; Ozer, 2000; Tulet et al., 2008; Laurent et al., 2008;  
227 Mokhtari, 2012; Hourdin et al., 2015). During this period, the studies of Dubovik et al. (2002); Schepanski et al. (2009b) or  
228 Tegen et al. (2013) suggested that the coarse mode fraction of mineral dust dominates the atmospheric mixture as AE values are  
229 below 0.7 (not shown) and are associated with AOD values greater than or equal to 0.3. Here, we have considered thresholds  
230 of 0.7 for AE and 0.2 for AOD to monitor the evolution of coarse (upper and lower bounds respectively) and fine (lower and  
231 upper bounds) modes of mineral aerosols.

232 Unlike winter, summer dust emissions are more concentrated in the higher layers of the ABL up to 6 km (Gamo, 1996) in  
233 response to intense convective mechanisms that are more common in the region at this season (Cuesta et al., 2009). Indeed, the  
234 convergence of hot, dry air (Harmatan) from the Sahara and fresh, moist air (monsoon) from the ocean causes the raising and  
235 maintenance of aerosol layers between 1 and 6 km at the thermal front area of the inter-tropical discontinuity (ITD) for which  
236 the northern edge is located around  $16^{\circ}\text{N}$  (Fig. 6c). Transport is also growing between 3 and 4 km above the ocean with a  
237 MDOF greater than 70%, i.e. more than 30% higher than that observed in DJF. This sharp increase of MDOF from DJF to JJA  
238 is in agreement with the results of (Schepanski et al., 2009b) who estimated an increase of more than 20% of the activity of dust  
239 sources in summer compared to winter in West Africa in the observations of Meteosat Second Generation (MSG) Spinning  
240 Enhanced Visible and Infrared Imager (SEVIRI). In summer, atmospheric dynamics raise large dust particles that are subject  
241 to the law of universal gravitation of Newton, thus settle much faster on the continent than the rest of the year. However, their  
242 reflectivity of solar radiation becomes larger and reaches a maximum value indicated by a SSA of 0.97 (Fig. 4c).

243 In autumn, SSA values are comparable to spring values but these high values are not due to high reflectance of desert aerosols  
244 like in spring because the southern migration of the Inter-Tropical Convergence Zone (ITCZ) reduces the activity of convective  
245 systems and causes a reduction of dust emissions shown by a decreasing of the AOD (Fig. 4d). These high SSA values can be





246 attributed to atmospheric conditions seen through the relative humidity which is much higher than in spring (Fig. 7d). Indeed,  
247 OMI measures the atmospheric properties of the aerosols which are known to be hygroscopic (Jethva et al., 2014).

#### 248 4.2 Continent-Ocean transition

249 To better understand the factors responsible for the high variability of the vertical transition of desert aerosols from the con-  
250 tinent to the ocean, we placed ourselves at a coastal point (Dakar) to study the variation of meteorological variables and their  
251 potential influence on the distribution of aerosols. Seasonality of vertical distributions of winds, relative humidity and potential  
252 temperature from radiosounding conducted at the weather station (GOOY) of Dakar (at West African shore) are shown in  
253 Figure. 7.

254 In DJF, continental winds are very strong at the surface with a maximum of 22 m/s at 500 m (Fig. 7a). The north-east direction  
255 of the winds in the first thousand meters explains the homogeneity of the vertical distribution of dust from the continent towards  
256 the ocean. Their intensity also explains the strong values of MDOF (up to 50%) observed by CALIOP in wintertime above the  
257 continent. Between 1 and 2 km height, winds weaken and change direction (south to south-east) while MDOF observed by  
258 satellite decreases (Fig. 5a). Between 2 and 5 km height, the winds turn to the southwest and west. These dust-depleted air  
259 masses of oceanic origin are wetter than from the land, and limit the development of the ABL. The air masses of continental  
260 origin are located between the surface and 2000 m height (Fig. 7a). In Figure. 7a, the relative humidity is around 20% (between  
261 500 and 2000 m) and it corresponds to a very dry air mass of Saharan origin. Between 2 and 5 km the potential temperature  
262 indicates a stable atmospheric layer.

263 Compared to the DJF situation, MAM surface winds (Fig. 7b) are intensifying to 25 m/s at 500 m height and are from the east.  
264 They are associated with MDOF above 50% in the ABL around 14°W. There is an inversion of easterly winds between 1 and  
265 3 km and a second southerly wind peak (15 m/s) appears between 3 and 4 km. It corresponds to the dust layer (SAL) detected  
266 by CALIOP. The vertical profile of potential temperature indicates a stable thick layer, well mixed between the surface and 3  
267 km (Fig. 7b). Beyond this altitude there is a stable stratification of the atmosphere indicated also by the potential temperature.  
268 Between 3 and 5 km height, the air masses coming from the South to the South-Southwest are also of oceanic origin and their  
269 interaction with a more consistent amount of dust than in winter could explain the better marked transition between the ocean  
270 and the continent in terms of SSA (increase) and AOD (decrease) for this season (Fig. 4b). Indeed, in general, increasing the  
271 relative humidity is likely to increase the SSA and size hygroscopic aerosols with dry to wet passage inducing a larger diameter  
272 even when humidity is below the saturation level (Hervo, 2013; Howell et al., 2006).

273 In JJA, surface winds (0-1 km) decrease and are from the West to the Southwest (West African Monsoon) (Fig. 7c). This  
274 corresponds to lower values of MDOF (Fig. 5c) but to relative humidity values well above DJF or MAM (Fig. 7). Reid et al.  
275 (2002) presented a conceptual model of Saharan dust transport in the middle troposphere describing an evolution of relative  
276 humidity profile in agreement with the observations made in Dakar. These authors describe a moistening of the surface layers  
277 due to monsoon flow which penetrates up to 1.5 km above this layer. Between 2 and 6 km, winds are from the East and above  
278 15 m/s. These wind velocity maxima reach 25 m/s in the range 3.5-5 km and are associated to the African Easterly Jet (AEJ)  
279 (Wu et al., 2009; Lafore et al., 2011). The co-localization of the AEJ and the SAL between 2 and 5 km height (Fig. 5c and



280 Fig. 7c) causes the westward SAL transport by AEJ in summer (Karyampudi et al., 1999). These strong winds correspond to  
281 the layer of dust detected by satellite at this altitude (Fig. 5c). Above the continent, the mesoscale features associated with  
282 the convergence between Harmattan and the West African Monsoon at the ITCZ cause strong updrafts that allow lifting and  
283 transport of dust particles throughout the air column (Tulet et al., 2008). The dynamics of the monsoon described by the con-  
284 ceptual scheme of mechanisms controlling the dust vertical redistribution in Cuesta et al. (2009) explain the wide occurrence  
285 of dust found between 2 and 5 km rather than at the surface. During transport from North Africa to the Atlantic Ocean, very  
286 large amounts of coarse dust (Fig. 4c) are deposited along the path with a rapid change in the size distribution of aerosols near  
287 the west African coast (Ryder et al., 2013). The signing of the SAL is evidenced by relative dryness of the atmosphere (Dulac  
288 et al., 2001) between 1.5 and 5 km (Fig. 7c). At this altitude, the vertical profile of potential temperature indicates Saharan  
289 origin of air masses with temperatures between 35°C and 45°C (Carlson and Prospero, 1972). The wind direction (east) given  
290 in Figure. 7c between 1.5 and 5 km altitude confirms the origin of the Saharan air masses. The presence of dust in the SAL  
291 causes both warming and drying of the atmosphere between 1.5 and 5 km and a cooling below this layer (Tulet et al., 2008).  
292 In SON, winds are weak and from the East at the surface (Fig. 7c). Between 1 and 5 km, it is increasing but is less intense than  
293 in JJA between 3 and 5 km and it is associated with a decrease of the MDOF (Fig. 5d). The moisture profile in SON (Fig. 7d)  
294 is close to that of JJA, but has a more humid atmosphere in the layer between 1.5 and 5 km where maximum relative humidity  
295 of the year occurs (60%; Fig. 7d). The analysis of the vertical distribution of thermodynamic variables like relative humidity,  
296 potential temperature and wind measured at the Dakar weather station shows that the thermodynamical conditions control the  
297 dust vertical distribution as well as the depth of the dust layer depending on the season. This analysis also explains the unintu-  
298 itive differences between spring, when the low values of SSA are associated with a strong AOD, and autumn characterized by  
299 high values of SSA associated with comparable AOD.

## 300 5 Conclusions

301 Studies of processes involved in the vertical distribution of aerosols at the transition between continent and ocean are very rare.  
302 Here, we took advantage of a weather station ideally located on the main pathway of desert aerosols from Northern Africa  
303 (Léon et al., 2009; Marticorena et al., 2010; Mortier et al., 2016) to explain the effect of meteorological variables on this transi-  
304 tion in a region of primary importance worldwide. The interaction of air masses of oceanic origin with dust aerosols are crucial  
305 for understanding their fate ( e.g., Friese et al., 2016). This study constitutes the first attempt to relate the seasonal dynamic  
306 of the atmosphere and the vertical distribution of dust aerosol in this region and provides the first dynamical explanation of a  
307 counterintuitive deposition pattern over the Atlantic ocean. Indeed, it explains the role of the local atmospheric circulation in  
308 driving a higher AOD and dust content in summer over west Africa in phase with dust deposition in Barbades islands but in  
309 opposition with Cape Verde islands where deposition is more intense in winter (Chiapello et al., 1995).  
310 We have studied the seasonal variability of the distribution of desert aerosols in West Africa (continental and oceanic) from  
311 their optical and physical properties. First of all we have been able to show a good estimate of physical properties (AOD  
312 and SSA) of aerosols by satellite when compared with AERONET ground measurements on the mainland, the coast and the



313 ocean. Space observations then allowed us to show the predominant presence of Saharan dust in the atmosphere north of 12°N  
314 throughout the year and an additional significant contribution of sandy sources from the Mauritanian coast in winter. The  
315 MDOF indicates a change in the vertical distribution of dust at the transition between the continent and the ocean, the largest  
316 differences occurring in spring and summer seasons. In DJF, the ABL is shallow ( $\sim 1$ km) and strong winds from North-East  
317 transport the dust in a dry atmosphere from the continent to the ocean continuously. This surface layer is superimposed by a  
318 stable atmospheric layer which inhibits the vertical development of this surface layer rich in dust aerosols. The decrease from  
319 east to west of the AOD requires material deposition during the transit. In summer, convection associated with structures that  
320 develop at the ITCZ distribute dust over 6 km height and create a thicker AOD. In the lower layers, the westward oceanic  
321 moistly entries which are opposite to the higher eastward winds generate very different distributions above the continent or the  
322 ocean. On the mainland, the dust is dominated by coarse mode and have a homogeneous vertical distribution while above the  
323 ocean, lower layers are poor in dust and are superimposed by the SAL which is highly enriched. The SSA remains constant at  
324 this transition. MAM and SON represent transition periods, MAM being closer to the summer situation.  
325 Future modeling experiments should bring further insights into ocean-atmosphere processes involved in explaining this transi-  
326 tion and the dust deposition along this pathway. It also seems that a more tailored approach to ocean-atmosphere interactions  
327 including higher frequencies of variability and notably the diurnal cycle is needed to make more apparent the role of local  
328 circulation on the vertical distribution of aerosols in coastal areas.

329 *Acknowledgements.* We would like to thank the IRD-BMBF AWA project and the international joint laboratory ECLAIRS for supporting  
330 and promoting our research activities. We thank the Institute of Research for Development for funding this PhD. We also thank ICARE for  
331 the online availability of the CALIPSO aerosol products at <http://www.icare.univ-lille1.fr/archive>. NCEP Reanalysis data were found online  
332 by the <http://www.esrl.noaa.gov/psd/data/gridded/data.ncep.reanalysis.pressure.html>, and the PIs and NASA for online AERONET data set  
333 which can be obtained from <http://aeronet.gsfc.nasa.gov/>. OMI aerosol products were downloaded at [http://disc.gsfc.nasa.gov/gesNews/  
334 giovanni\\_3\\_end\\_of\\_service?instance\\_id=omil2g&selectedMap=Blue%2520Marble&](http://disc.gsfc.nasa.gov/gesNews/giovanni_3_end_of_service?instance_id=omil2g&selectedMap=Blue%2520Marble&). We are finally very grateful to B. Marticorena and I.  
335 Chiapello for very fruitful discussions.



## 336 References

- 337 Adams, A. M., Prospero, J. M., and Zhang, C.: CALIPSO-derived three-dimensional structure of aerosol over the Atlantic Basin and adjacent  
338 continents, *Journal of Climate*, 25, 6862–6879, 2012.
- 339 Andreae, M. O. et al.: Raising dust in the greenhouse, *Nature*, 380, 389–390, 1996.
- 340 Aristegui, J., Barton, E. D., Álvarez-Salgado, X. A., Santos, A. M. P., Figueiras, F. G., Kifani, S., Hernández-León, S., Mason, E., Machú,  
341 E., and Demarcq, H.: Sub-regional ecosystem variability in the Canary Current upwelling, *Progress in Oceanography*, 83, 33–48, 2009.
- 342 Baker, A., Kelly, S., Biswas, K., Witt, M., and Jickells, T.: Atmospheric deposition of nutrients to the Atlantic Ocean, *Geophysical Research  
343 Letters*, 30, 2003.
- 344 Ben-Ami, Y., Koren, I., and Altaratz, O.: Patterns of North African dust transport over the Atlantic: winter vs. summer, based on CALIPSO  
345 first year data, *Atmospheric Chemistry and Physics*, 9, 7867–7875, 2009.
- 346 Ben-Ami, Y., Koren, I., Rudich, Y., Artaxo, P., Martin, S., and Andreae, M.: Transport of North African dust from the Bodélé depression to  
347 the Amazon Basin: a case study, *Atmospheric Chemistry and Physics*, 10, 7533–7544, 2010.
- 348 Bertrand, J., Cerf, A., and Domergue, J.: Repartition in space and time of dust haze south of the Sahara, *The Long-Range Transport of  
349 Pollutants and its Relation to Gen. Circulation Including Stratospheric/Tropospheric Exchange Processes* p 409-415(SEE N 80-26888  
350 17-45), 1979.
- 351 Bettenhausen, C. and Team, G. D. M.: Consistent Long-Term Aerosol Data Records over Land and Ocean from SeaWiFS, in: *Goddard Space  
352 Flight Center Greenbelt, Maryland*, pp. 1–19, <http://disc.sci.gsfc.nasa.gov/dust/documentation/README.DeepBlueSeaWiFS.pdf>, 2013.
- 353 Bou Karam, D., Flamant, C., Knippertz, P., Reitebuch, O., Pelon, J., Chong, M., and Dabas, A.: Dust emissions over the Sahel associated with  
354 the West African monsoon intertropical discontinuity region: A representative case-study, *Quarterly Journal of the Royal Meteorological  
355 Society*, 134, 621–634, 2008.
- 356 Braun, S. A.: Reevaluating the role of the Saharan air layer in Atlantic tropical cyclogenesis and evolution, *Monthly Weather Review*, 138,  
357 2007–2037, 2010.
- 358 Brooks, N. and Legrand, M.: Dust variability over northern Africa and rainfall in the Sahel, in: *Linking climate change to land surface  
359 change*, pp. 1–25, Springer, 2000.
- 360 Cakmur, R. V., Miller, R. L., and Tegen, I.: A comparison of seasonal and interannual variability of soil dust aerosols over the Atlantic Ocean  
361 as inferred by the TOMS AI and AVHRR AOT retrievals, *Journal of Geophysical Research: Atmospheres*, 106, 18 287–18 303, 2001.
- 362 Carlson, T. N. and Prospero, J. M.: The large-scale movement of Saharan air outbreaks over the northern equatorial Atlantic, *Journal of  
363 applied meteorology*, 11, 283–297, 1972.
- 364 Cavalieri, O., Cairo, F., Fierli, F., Donfrancesco, G. D., Snels, M., Viterbini, M., Cardillo, F., Chatenet, B., Formenti, P., Marticorena, B.,  
365 et al.: Variability of aerosol vertical distribution in the Sahel, *Atmospheric Chemistry and Physics*, 10, 12 005–12 023, 2010.
- 366 Chiapello, I. and Moulin, C.: TOMS and METEOSAT satellite records of the variability of Saharan dust transport over the Atlantic during  
367 the last two decades (1979–1997), *Geophysical Research Letters*, 29, 2002.
- 368 Chiapello, I., Bergametti, G., Gomes, L., Chatenet, B., Dulac, F., Pimenta, J., and Santos Soares, E.: An additional low layer transport of  
369 Sahelian and Saharan dust over the north-eastern tropical Atlantic, *Geophysical Research Letters*, 22, 3191–3194, 1995.
- 370 Chiapello, I., Prospero, J., Herman, J., and Hsu, N.: Detection of mineral dust over the North Atlantic Ocean and Africa with the Nimbus 7  
371 TOMS, *Journal of Geophysical Research: Atmospheres*, 104, 9277–9291, 1999.



- 372 Chou, C., Formenti, P., Maille, M., Ausset, P., Helas, G., Osborne, S., and Harrison, M.: Size distribution, shape and composition of dust  
373 aerosols collected during the AMMA SOP0 field campaign in the northeast of Niger, January 2006, *J. Geophys. Res.*, 113, D00C10, 2008.
- 374 Claquin, T., Schulz, M., and Balkanski, Y.: Modeling the mineralogy of atmospheric dust sources, *Journal of Geophysical Research: Atmo-*  
375 *spheres*, 104, 22 243–22 256, 1999.
- 376 Cuesta, J., Marsham, J. H., Parker, D. J., and Flamant, C.: Dynamical mechanisms controlling the vertical redistribution of dust and the  
377 thermodynamic structure of the West Saharan atmospheric boundary layer during summer, *Atmospheric Science Letters*, 10, 34–42, 2009.
- 378 Diokhane, A. M., Jenkins, G. S., Manga, N., Drame, M. S., and Mbodji, B.: Linkages between observed, modeled Saharan dust loading and  
379 meningitis in Senegal during 2012 and 2013, *International journal of biometeorology*, 60, 557–575, 2016.
- 380 Dubovik, O., Smirnov, A., Holben, B., King, M., Kaufman, Y., Eck, T., and Slutsker, I.: Accuracy assessments of aerosol optical properties re-  
381 trieved from Aerosol Robotic Network (AERONET) Sun and sky radiance measurements, *Journal of Geophysical Research: Atmospheres*,  
382 105, 9791–9806, 2000.
- 383 Dubovik, O., Holben, B., Eck, T. F., Smirnov, A., Kaufman, Y. J., King, M. D., Tanré, D., and Slutsker, I.: Variability of absorption and  
384 optical properties of key aerosol types observed in worldwide locations, *Journal of the atmospheric sciences*, 59, 590–608, 2002.
- 385 Duce, R. A. and Tindale, N. W.: Atmospheric transport of iron and its deposition in the ocean, *Limnology and Oceanography*, 36, 1715–1726,  
386 1991.
- 387 Dulac, F., Chazette, P., Gomes, L., Chatenet, B., Berger, H., and Dos Santos, J. V.: A method for aerosol profiling in the lower troposphere  
388 with coupled scatter and meteorological rawinsondes and first data from the tropical Atlantic off Sahara, *Journal of aerosol science*, 32,  
389 1069–1086, 2001.
- 390 Dunion, J. P. and Marron, C. S.: A reexamination of the Jordan mean tropical sounding based on awareness of the Saharan air layer: Results  
391 from 2002, *Journal of Climate*, 21, 5242–5253, 2008.
- 392 Engelstaedter, S., Tegen, I., and Washington, R.: North African dust emissions and transport, *Earth-Science Reviews*, 79, 73–100, 2006.
- 393 Eplee, R. E., Patt, F. S., Barnes, R. A., and McClain, C. R.: SeaWiFS long-term solar diffuser reflectance and sensor noise analyses, *Applied*  
394 *optics*, 46, 762–773, 2007.
- 395 Eplee Jr, R. E., Sun, J.-Q., Meister, G., Patt, F. S., Xiong, X., and McClain, C. R.: Cross calibration of SeaWiFS and MODIS using on-orbit  
396 observations of the Moon, *Applied Optics*, 50, 120–133, 2011.
- 397 Formenti, P., Rajot, J. L., Desboeufs, K., Caquineau, S., Chevaillier, S., Nava, S., Gaudichet, A., Journet, E., Triquet, S., Alfaro, S., et al.:  
398 Regional variability of the composition of mineral dust from western Africa: Results from the AMMA SOP0/DABEX and DODO field  
399 campaigns, *Journal of Geophysical Research: Atmospheres*, 113, 2008.
- 400 Franz, B. A., Bailey, S. W., Werdell, P. J., and McClain, C. R.: Sensor-independent approach to the vicarious calibration of satellite ocean  
401 color radiometry, *Applied optics*, 46, 5068–5082, 2007.
- 402 Friese, C. A., van der Does, M., Merkel, U., Iversen, M. H., Fischer, G., and Stuut, J.-B. W.: Environmental factors controlling the seasonal  
403 variability in particle size distribution of modern Saharan dust deposited off Cape Blanc, *Aeolian Research*, 22, 165–179, 2016.
- 404 Gamo, M.: Thickness of the dry convection and large-scale subsidence above deserts, *Boundary-Layer Meteorology*, 79, 265–278, 1996.
- 405 Generoso, S., Bey, I., Labonne, M., and Bréon, F.-M.: Aerosol vertical distribution in dust outflow over the Atlantic: Comparisons between  
406 GEOS-Chem and Cloud-aerosol Lidar and Infrared Pathfinder Satellite Observation (CALIPSO), *Journal of Geophysical Research: At-*  
407 *mospheres*, 113, 2008.
- 408 Griffin, D. W.: Atmospheric movement of microorganisms in clouds of desert dust and implications for human health, *Clinical microbiology*  
409 *reviews*, 20, 459–477, 2007.



- 410 Heese, B. and Wiegner, M.: Vertical aerosol profiles from Raman polarization lidar observations during the dry season AMMA field cam-  
411 paign, *Journal of Geophysical Research: Atmospheres*, 113, 2008.
- 412 Hervo, M.: Etude des propriétés optiques et radiatives des aérosols en atmosphère réelle: Impact de l'hygroscopicité, Ph.D. thesis, Université  
413 Blaise Pascal-Clermont-Ferrand II, 2013.
- 414 Holben, B., Tanre, D., Smirnov, A., Eck, T., Slutsker, I., Abuhassan, N., Newcomb, W., Schafer, J., Chatenet, B., Lavenu, F., et al.: An  
415 emerging ground-based aerosol climatology: Aerosol optical depth from AERONET, *Journal of Geophysical Research: Atmospheres*,  
416 106, 12 067–12 097, 2001.
- 417 Holben, B. N., Eck, T., Slutsker, I., Tanre, D., Buis, J., Setzer, A., Vermote, E., Reagan, J. A., Kaufman, Y., Nakajima, T., et al.:  
418 AERONET—A federated instrument network and data archive for aerosol characterization, *Remote sensing of environment*, 66, 1–16,  
419 1998.
- 420 Hourdin, F., Gueye, M., Diallo, B., Dufresne, J.-L., Escribano, J., Menut, L., Marticoréna, B., Siour, G., and Guichard, F.: Parameterization  
421 of convective transport in the boundary layer and its impact on the representation of the diurnal cycle of wind and dust emissions,  
422 *Atmospheric Chemistry and Physics*, 15, 6775–6788, 2015.
- 423 Howell, S., Clarke, A., Shinozuka, Y., Kapustin, V., McNaughton, C., Huebert, B., Doherty, S., and Anderson, T.: Influence of relative  
424 humidity upon pollution and dust during ACE-Asia: Size distributions and implications for optical properties, *Journal of Geophysical*  
425 *Research: Atmospheres*, 111, 2006.
- 426 Hsu, N., Gautam, R., Sayer, A., Bettenhausen, C., Li, C., Jeong, M., Tsay, S., and Holben, B.: Global and regional trends of aerosol optical  
427 depth over land and ocean using SeaWiFS measurements from 1997 to 2010, 2012.
- 428 Hsu, N. C., Tsay, S.-C., King, M. D., and Herman, J. R.: Aerosol properties over bright-reflecting source regions, *IEEE Transactions on*  
429 *Geoscience and Remote Sensing*, 42, 557–569, 2004.
- 430 Hunt, W. H., Winker, D. M., Vaughan, M. A., Powell, K. A., Lucker, P. L., and Weimer, C.: CALIPSO lidar description and performance  
431 assessment, *Journal of Atmospheric and Oceanic Technology*, 26, 1214–1228, 2009.
- 432 Husar, R. B., Prospero, J. M., and Stowe, L. L.: Characterization of tropospheric aerosols over the oceans with the NOAA advanced very high  
433 resolution radiometer optical thickness operational product, *Journal of Geophysical Research: Atmospheres*, 102, 16 889–16 909, 1997.
- 434 Ialongo, I., Buchard, V., Brogniez, C., Casale, G., and Siani, A.: Aerosol Single Scattering Albedo retrieval in the UV range: an application  
435 to OMI satellite validation, *Atmospheric Chemistry and Physics*, 10, 331–340, 2010.
- 436 Jamet, C., Moulin, C., and Thiria, S.: Monitoring aerosol optical properties over the Mediterranean from SeaWiFS images using a neural  
437 network inversion, *Geophysical Research Letters*, 31, 2004.
- 438 Jethva, H., Torres, O., and Ahn, C.: Global assessment of OMI aerosol single-scattering albedo using ground-based AERONET inversion,  
439 *Journal of Geophysical Research: Atmospheres*, 119, 9020–9040, 2014.
- 440 Jickells, T., An, Z., Andersen, K. K., Baker, A., Bergametti, G., Brooks, N., Cao, J., Boyd, P., Duce, R., Hunter, K., et al.: Global iron  
441 connections between desert dust, ocean biogeochemistry, and climate, *science*, 308, 67–71, 2005.
- 442 Johnson, B., Osborne, S., Haywood, J., and Harrison, M.: Aircraft measurements of biomass burning aerosol over West Africa during  
443 DABEX, *Journal of Geophysical Research: Atmospheres*, 113, 2008.
- 444 Joseph, M.: Long-term measurements of the transport of African mineral dust to the southeastern United States: Implications for regional air  
445 quality, 1999.
- 446 Karyampudi, V. M., Palm, S. P., Reagen, J. A., Fang, H., et al.: Validation of the Saharan dust plume conceptual model using lidar, Meteosat,  
447 and ECMWF data, *Bulletin of the American Meteorological Society*, 80, 1045, 1999.





- 448 Kaufman, Y., Koren, I., Remer, L., Tanré, D., Ginoux, P., and Fan, S.: Dust transport and deposition observed from the Terra-Moderate  
449 Resolution Imaging Spectroradiometer (MODIS) spacecraft over the Atlantic Ocean, *Journal of Geophysical Research: Atmospheres*,  
450 110, 2005.
- 451 Lafore, J.-P., Flamant, C., Guichard, F., Parker, D., Bouniol, D., Fink, A., Giraud, V., Gosset, M., Hall, N., Höller, H., et al.: Progress in  
452 understanding of weather systems in West Africa, *Atmospheric Science Letters*, 12, 7–12, 2011.
- 453 Laurent, B., Marticorena, B., Bergametti, G., Léon, J., and Mahowald, N.: Modeling mineral dust emissions from the Sahara desert using  
454 new surface properties and soil database, *Journal of Geophysical Research: Atmospheres*, 113, 2008.
- 455 Léon, J.-F., Derimian, Y., Chiapello, I., Tanré, D., Podvin, T., Chatenet, B., Diallo, A., and Deroo, C.: Aerosol vertical distribution and optical  
456 properties over M’ Bour (16.96 W; 14.39 N), Senegal from 2006 to 2008, *Atmospheric Chemistry and Physics*, 9, 9249–9261, 2009.
- 457 Levelt, P. F., van den Oord, G. H., Dobber, M. R., Malkki, A., Visser, H., de Vries, J., Stammes, P., Lundell, J. O., and Saari, H.: The ozone  
458 monitoring instrument, *IEEE Transactions on geoscience and remote sensing*, 44, 1093–1101, 2006.
- 459 Liu, D., Wang, Z., Liu, Z., Winker, D., and Trepte, C.: A height resolved global view of dust aerosols from the first year CALIPSO lidar  
460 measurements, *Journal of Geophysical Research: Atmospheres*, 113, 2008.
- 461 Liu, D., Wang, Y., Wang, Z., and Zhou, J.: The three-dimensional structure of transatlantic African dust transport: a new perspective from  
462 CALIPSO LIDAR measurements, *Advances in Meteorology*, 2012, 2012.
- 463 Liu, Z., Omar, A., Hu, Y., Vaughan, M., Winker, D., Poole, L., and Kovacs, T.: CALIOP algorithm theoretical basis document. Part 3: Scene  
464 classification algorithms, NASA-CNES document PC-SCI-203, 2005.
- 465 Mahowald, N. M., Engelstaedter, S., Luo, C., Sealy, A., Artaxo, P., Benitez-Nelson, C., Bonnet, S., Chen, Y., Chuang, P. Y., Cohen, D. D.,  
466 et al.: Atmospheric Iron Deposition: Global Distribution, Variability, and Human Perturbations\*, *Annual Review of Marine Science*, 1,  
467 245–278, 2009.
- 468 Malavelle, F.: Effets direct et semi-direct des aérosols en Afrique de l’ouest pendant la saison sèche, Ph.D. thesis, Université Paul Sabatier-  
469 Toulouse III, 2011.
- 470 Marticorena, B., Chatenet, B., Rajot, J.-L., Traoré, S., Coulibaly, M., Diallo, A., Koné, I., Maman, A., NDiaye, T., and Zakou, A.: Temporal  
471 variability of mineral dust concentrations over West Africa: analyses of a pluriannual monitoring from the AMMA Sahelian Dust Transect,  
472 *Atmospheric Chemistry and Physics*, 10, 8899–8915, 2010.
- 473 Martin, J. H.: Iron as a limiting factor in oceanic productivity, in: *Primary productivity and biogeochemical cycles in the sea*, pp. 123–137,  
474 Springer, 1992.
- 475 Martiny, N. and Chiapello, I.: Assessments for the impact of mineral dust on the meningitis incidence in West Africa, *Atmospheric Environ-*  
476 *ment*, 70, 245–253, 2013.
- 477 Mielonen, T., Arola, A., Komppula, M., Kukkonen, J., Koskinen, J., de Leeuw, G., and Lehtinen, K.: Comparison of CALIOP level 2 aerosol  
478 subtypes to aerosol types derived from AERONET inversion data, *Geophysical Research Letters*, 36, 2009.
- 479 Mills, M. M., Ridame, C., Davey, M., La Roche, J., and Geider, R. J.: Iron and phosphorus co-limit nitrogen fixation in the eastern tropical  
480 North Atlantic, *Nature*, 429, 292–294, 2004.
- 481 Mokhtari, M.: Amélioration de la prise en compte des aérosols terrigènes dans les modèles atmosphériques à moyenne échelle, Ph.D. thesis,  
482 Université de Toulouse, Université Toulouse III-Paul Sabatier, 2012.
- 483 Mortier, A., Goloub, P., Derimian, Y., Tanré, D., Podvin, T., Blarel, L., Deroo, C., Marticorena, B., Diallo, A., and Ndiaye, T.: Climatology  
484 of aerosol properties and clear-sky shortwave radiative effects using Lidar and Sun photometer observations in the Dakar site, *Journal of*  
485 *Geophysical Research: Atmospheres*, 2016.



- 486 Moulin, C.: Transport atmosphérique des poussières africaines sur la Méditerranée et l'Atlantique: climatologie satellitale à partir des images  
487 Météosat VIS(1983-1994) et relations avec le climat, Ph.D. thesis, 1997.
- 488 Omar, A. H., Winker, D. M., Vaughan, M. A., Hu, Y., Trepte, C. R., Ferrare, R. A., Lee, K.-P., Hostetler, C. A., Kittaka, C., Rogers, R. R.,  
489 et al.: The CALIPSO automated aerosol classification and lidar ratio selection algorithm, *Journal of Atmospheric and Oceanic Technology*,  
490 26, 1994–2014, 2009.
- 491 Ozer, P.: Les lithométéores en région sahélienne: un indicateur climatique de la désertification, Ph.D. thesis, Université de Liège Faculté des  
492 sciences Liège Belgique, Liège, Belgique, 2000.
- 493 Petzold, A., Veira, A., Mund, S., Esselborn, M., Kiemle, C., Weinzierl, B., Hamburger, T., Ehret, G., Lieke, K., and Kandler, K.: Mixing of  
494 mineral dust with urban pollution aerosol over Dakar (Senegal): impact on dust physico-chemical and radiative properties, *Tellus B*, 63,  
495 619–634, 2011.
- 496 Prospero, J., Glaccum, R., and Nees, R.: Atmospheric transport of soil dust from Africa to South America, *Nature*, 289, 570–572, 1981.
- 497 Prospero, J. M., Blades, E., Mathison, G., and Naidu, R.: Interhemispheric transport of viable fungi and bacteria from Africa to the Caribbean  
498 with soil dust, *Aerobiologia*, 21, 1–19, 2005.
- 499 Rajot, J.-L.: Wind blown sediment mass budget of Sahelian village land units in Niger, *Bulletin de la Société Géologique de France*, 172,  
500 523–531, 2001.
- 501 Ramanathan, V., Crutzen, P., Kiehl, J., and Rosenfeld, D.: Aerosols, climate, and the hydrological cycle, *science*, 294, 2119–2124, 2001.
- 502 Reid, J. S., Westphal, D. L., Livingston, J. M., Savoie, D. L., Maring, H. B., Jonsson, H. H., Eleuterio, D. P., Kinney, J. E., and Reid, E. A.:  
503 Dust vertical distribution in the Caribbean during the Puerto Rico Dust Experiment, *Geophysical research letters*, 29, 2002.
- 504 Ridley, D., Heald, C., and Ford, B.: North African dust export and deposition: A satellite and model perspective, *Journal of Geophysical*  
505 *Research: Atmospheres*, 117, 2012.
- 506 Ryder, C., Highwood, E., Lai, T., Sodemann, H., and Marsham, J.: Impact of atmospheric transport on the evolution of microphysical and  
507 optical properties of Saharan dust, *Geophysical Research Letters*, 40, 2433–2438, 2013.
- 508 Sayer, A., Hsu, N., Bettenhausen, C., Ahmad, Z., Holben, B., Smirnov, A., Thomas, G., and Zhang, J.: SeaWiFS Ocean Aerosol Retrieval  
509 (SOAR): Algorithm, validation, and comparison with other data sets, *Journal of Geophysical Research: Atmospheres*, 117, 2012.
- 510 Schepanski, K., Tegen, I., and Macke, A.: Saharan dust transport and deposition towards the tropical northern Atlantic, *Atmos. Chem. Phys.*,  
511 9, 1173–1189, 2009a.
- 512 Schepanski, K., Tegen, I., Todd, M., Heinold, B., Bönisch, G., Laurent, B., and Macke, A.: Meteorological processes forcing Saharan dust  
513 emission inferred from MSG-SEVIRI observations of subdaily dust source activation and numerical models, *Journal of Geophysical*  
514 *Research: Atmospheres*, 114, 2009b.
- 515 Slutsker, I. and Kinne, S.: Wavelength dependence of the optical depth of biomass burning, urban, and desert dust aerosols, *J Geophys Res.*,  
516 104, 00093–5, 1999.
- 517 Sokolik, I. N. and Toon, O. B.: Incorporation of mineralogical composition into models of the radiative properties of mineral aerosol from  
518 UV to IR wavelengths, *Journal of Geophysical Research*, 104, 9423–9444, 1999.
- 519 Solomon, S.: *Climate change 2007-the physical science basis: Working group I contribution to the fourth assessment report of the IPCC*,  
520 vol. 4, Cambridge University Press, 2007.
- 521 Stith, J., Ramanathan, V., Cooper, W., Roberts, G., DeMott, P., Carmichael, G., Hatch, C., Adhikary, B., Twohy, C., Rogers, D., et al.: An  
522 overview of aircraft observations from the Pacific Dust Experiment campaign, *Journal of Geophysical Research: Atmospheres*, 114, 2009.



- 523 Tanaka, T. Y., Kurosaki, Y., Chiba, M., Matsumura, T., Nagai, T., Yamazaki, A., Uchiyama, A., Tsunematsu, N., and Kai, K.: Possible  
524 transcontinental dust transport from North Africa and the Middle East to East Asia, *Atmospheric Environment*, 39, 3901–3909, 2005.
- 525 Tegen, I., Schepanski, K., and Heinold, B.: Comparing two years of Saharan dust source activation obtained by regional modelling and  
526 satellite observations, *Atmospheric Chemistry and Physics*, 13, 2381–2390, 2013.
- 527 Teller, A. and Levin, Z.: The effects of aerosols on precipitation and dimensions of subtropical clouds: a sensitivity study using a numerical  
528 cloud model, *Atmospheric Chemistry and Physics*, 6, 67–80, 2006.
- 529 Thomson, M. C., Molesworth, A. M., Djingarey, M. H., Yameogo, K., Belanger, F., and Cuevas, L. E.: Potential of environmental models to  
530 predict meningitis epidemics in Africa, *Tropical Medicine & International Health*, 11, 781–788, 2006.
- 531 Tsamalis, C., Chédin, A., Pelon, J., and Capelle, V.: The seasonal vertical distribution of the Saharan Air Layer and its modulation by the  
532 wind, *Atmospheric Chemistry and Physics*, 13, 11 235–11 257, 2013.
- 533 Tulet, P., Mallet, M., Pont, V., Pelon, J., and Boone, A.: The 7–13 March 2006 dust storm over West Africa: Generation, transport, and  
534 vertical stratification, *Journal of Geophysical Research: Atmospheres*, 113, 2008.
- 535 Vuolo, M. R., Chepfer, H., Menut, L., and Cesana, G.: Comparison of mineral dust layers vertical structures modeled with CHIMERE-DUST  
536 and observed with the CALIOP lidar, *Journal of Geophysical Research: Atmospheres*, 114, 2009.
- 537 Wagener, T.: Le fer à l'interface océan-atmosphère: Flux et processus de dissolution dans l'eau de mer., Ph.D. thesis, Université de la  
538 Méditerranée-Aix-Marseille II, 2008.
- 539 Wang, M., Bailey, S., Pietras, C., McClain, C., and Riley, T.: SeaWiFS aerosol optical thickness matchup analyses, *The Sea-WiFS Postlaunch*  
540 *Technical Report Series*, 10, 39–44, 2000.
- 541 Winker, D.: Accounting for multiple scattering in retrievals from space lidar, in: *Proc. of SPIE Vol.*, vol. 5059, p. 129, 2003.
- 542 Winker, D. M., Hostetler, C., Vaughan, M., and Omar, A.: CALIOP Algorithm Theoretical Basis Document, Part 1: CALIOP Instrument,  
543 and Algorithms Overview, Release, 2, 29, 2006.
- 544 Winker, D. M., Hunt, W. H., and McGill, M. J.: Initial performance assessment of CALIOP, *Geophysical Research Letters*, 34, 2007.
- 545 Wu, M.-L. C., Reale, O., Schubert, S. D., Suarez, M. J., Koster, R. D., and Pegion, P. J.: African easterly jet: structure and maintenance,  
546 *Journal of Climate*, 22, 4459–4480, 2009.
- 547 Yang, W., Marshak, A., Várnai, T., Kalashnikova, O. V., and Kostinski, A. B.: CALIPSO observations of transatlantic dust: vertical stratifi-  
548 cation and effect of clouds, *Atmospheric Chemistry and Physics*, 12, 11 339–11 354, 2012.
- 549 Yu, H., Chin, M., Winker, D. M., Omar, A. H., Liu, Z., Kittaka, C., and Diehl, T.: Global view of aerosol vertical distributions from CALIPSO  
550 lidar measurements and GOCART simulations: Regional and seasonal variations, *Journal of Geophysical Research: Atmospheres*, 115,  
551 2010.

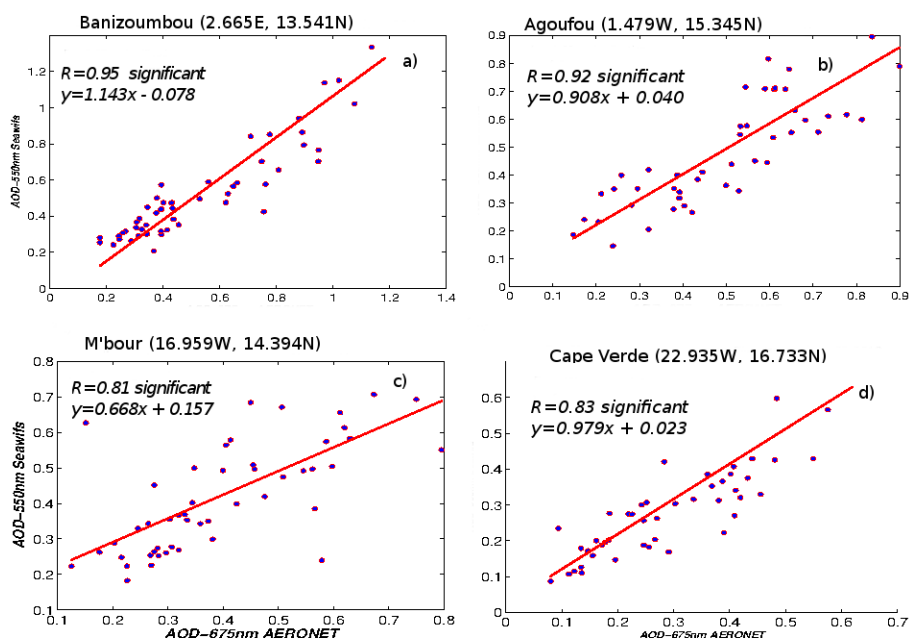


**Figure 1.** Comparison of monthly mean aerosol optical depth (AOD) between SeaWiFS (550 nm) and ground measurements from AERONET (675 nm) from January 2005 to December 2010. This comparison is done at the following stations : a) Banizoumbou (53 points), b) Agoufou (47 points), c) M'bour (50 points) and d) Cape verde (47 points). The red solid line represents the regression between both dataset

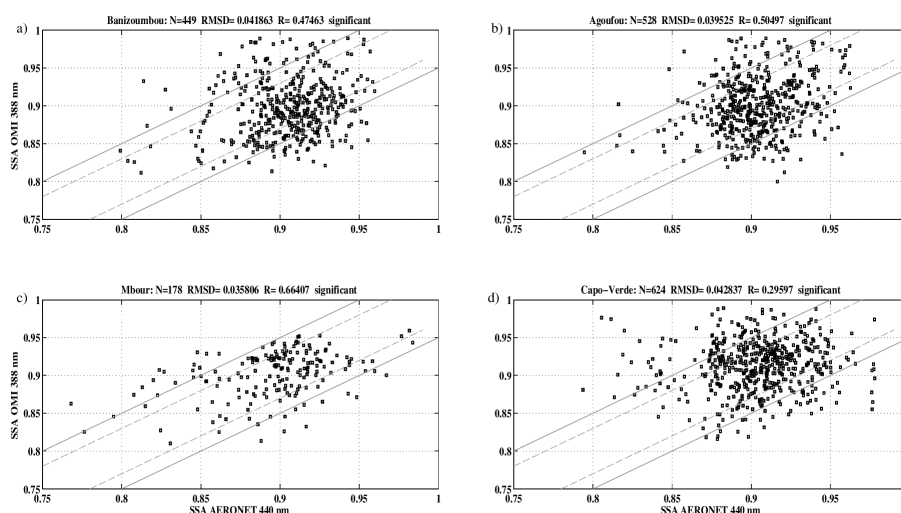


**Figure 2.** OMAERUV SSA at 440 nm wavelength as a function of AERONET SSA at 440 nm at a) Banizoumbou (lon=2.665, lat=13.541; a total of 449 retrievals are plotted, yielding a root mean square difference (RMSD) of 0.04); b) Agoufou (lon=-1.479, lat=15.345; 528 retrievals with a RMSD of 0.04); c) Mbour (lon=-16.959, lat=14.394; 178 retrievals with a RMSD of 0.04) and d) Capo Verde (lon=-22.935, lat=16.733; 624 retrievals with a RMSD of 0.04). The solid lines indicate the domain where the two retrievals agree with each other within 0.03 and the dashed lines indicate agreement within 0.05. The AERONET's data used here are Level 2, quality assured for Banizoumbou, Agoufou and M'bour sites. For Cape Verde Level 1.5, is used to get a significant number of retrievals.

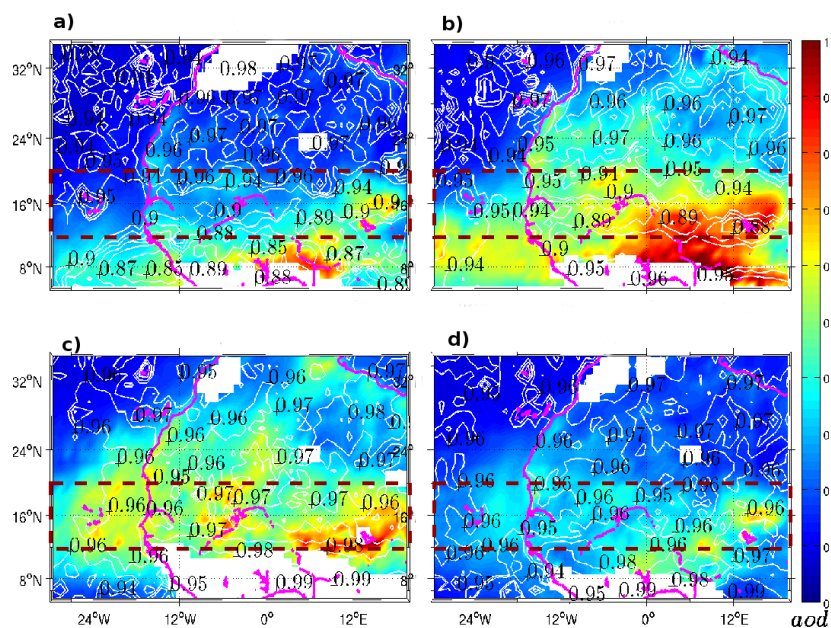


**Figure 3.** Seasonal distribution of aerosol optical depth (average between 2005 and 2010) at 550 nm wavelength (colours) from SeaWiFS for a) winter (DJF); b) spring (MAM); c) summer (JJA) and d) fall (SON). Single scattering albedo (SSA) from OMI is superimposed with white contour lines. The box delimited by brown dashed lines represent the band of latitude averaged in Fig. 4 (12°-21°N) where dust aerosols have the strongest contribution to AOD.

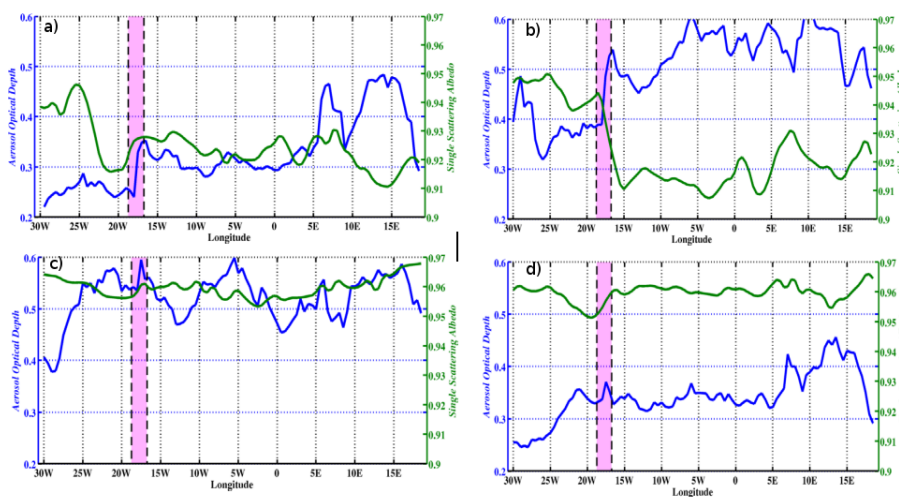


**Figure 4.** Seasonal SeaWiFS AOD at 550 nm (bleu), Aura/OMI SSA (green) zonally averaged between 12° and 21°N and from 2005 to 2010: a) DJF; b) MAM; c) JJA; and d) SON. The black dashed lines indicate the continent-ocean transition for the latitude range 12°-21°N.



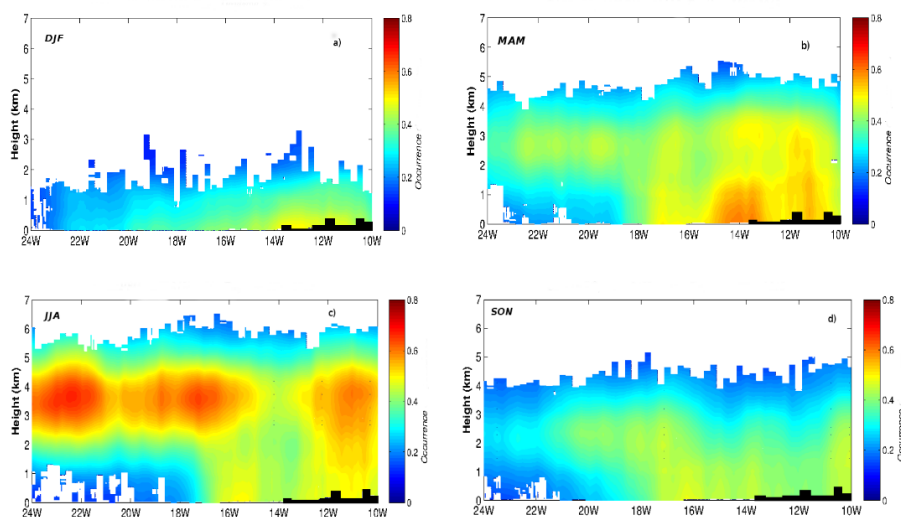


**Figure 5.** CALIOP daytime seasonal vertical distribution of the frequency of mineral dust aerosol occurrence zonally averaged between 12° and 21°N over the period 2007-2013: a) winter; b) spring; c) summer; and d) fall.

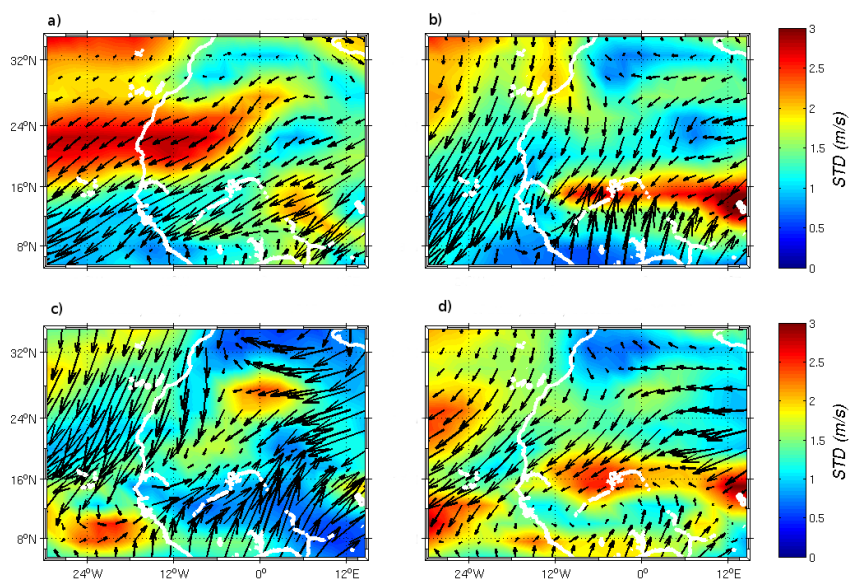


**Figure 6.** Seasonal mean zonal wind field at 925 hPa over West Africa from NCEP Reanalysis between 2000 and 2012: a) winter (DJF); b) spring (MAM); c) summer (JJA); and d) fall (SON). The vectors show wind direction while colors indicate the standard deviation of wind velocity ( $\text{m}\cdot\text{s}^{-1}$ ).

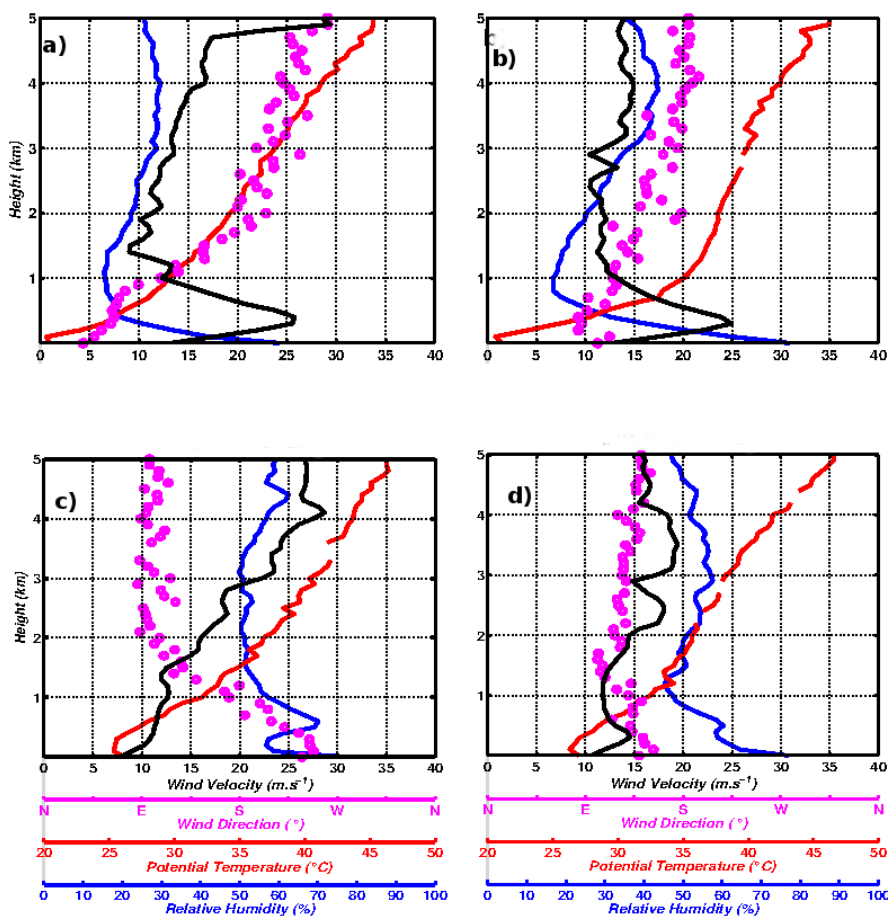


**Figure 7.** Mean seasonal vertical profiles of wind velocity (black line), wind direction (pink dots), potential temperature (red line) and relative humidity (blue line) at Dakar weather station (14.73°N, 17.51°W) for a) winter; b) spring; c) summer; and d) fall. Observations correspond to weather balloon launched daily at 12UTC for years 2012 to 2014.